Measurement of Laser-Induced Plasma: Stark Broadening Parameters of Pb(II) 2203.5 and 4386.5 Å Spectral Lines

Aurelia Alonso Medina

Abstract

In this work, the Stark broadening parameters (widths and shifts) of the 2203.5 Å and 4386.5 Å Pb(II) spectral lines have been investigated and measured in laser-induced breakdown spectroscopy (LIBS), using a lead sample (99.999% purity). A Q-switched neodymium-doped yttrium aluminum garnet (Nd:YAG) laser operating at its fundamental wavelength (10 640 Å), generating pulses of 290 mJ, 7 ns of duration, and a repeat frequency of 20 Hz, has been used for the ablation of said lead sample in vacuum and in a controlled argon atmosphere. A study to understand the expansion dynamics of the lead produced plasma was performed. The spectra have been obtained and measured at different time delays of the plasma evolution in the range of 0.15–9 μs, at which the temperature and electron number density are in the ranges of 28 200–8000 K and 1.3×10^{17} to 3×10^{15} cm^{-3}, respectively. A graphical representation of the evolution of temperature and electron number density versus 0.3 to 6.5 μs delay from the laser pulse is presented. The important effect of the different environment where the plasma expands has been pointed out. Local thermodynamic equilibrium conditions have been checked. The obtained results of the Stark widths and shifts at the different temperatures and densities of electrons have been compared with the limited data available in the literature. This study aims to obtain more accurate values for these parameters and also to establish regularities and similarities for said parameters.

Introduction

The data of Stark broadening parameters (widths and shifts) of the spectral lines are of interest in atomic structure studies, as well as for plasma diagnostics in different fields ranging from laboratory to analytical chemistry and are vital in astrophysics; these parameters are important to verify stellar evolution models. Lead is the heaviest element thus far detected in the interstellar medium; Pb(II) has been detected in several stars with the Goddard High Resolution Spectrograph (GHRS) aboard the Hubble Space Telescope (HST).[1] Lead is one of the most exploited elements in the various fields of the industry and technology. It is also one of the most important metals and is a well-known toxin, used in metallurgy, paper and pulp industries, metal products, etc. Lead is a major harmful pollutant to the biosphere: it is a hazardous pollutant that leads to severe ecological problems and has a toxic effect on living organisms.[2] Lead exists as Pb(II) in water that enters into food chains and accumulates in the soft tissues of the body. The line of Pb(II) 2203.5 Å is one of the lines that is taken as a target line to verify the limit of detection (LOD) of the lead element of interest.[3,4] The determination of contaminant elements in water is important for many applications, such as monitoring polluting elements in effluent streams of industrial processes or quality control;[5,6] laser-induced breakdown spectroscopy (LIBS) is the ideal tool for this purpose.

Experimental data for Stark widths and shifts of 2203.5 Å and 4386.5 Å Pb(II) spectral lines are scarce in the literature. In 1979, Miller et al.[7] obtained experimental Stark half-widths of seven visible (4152.8 Å, 4245.1 Å, 4386.4 Å, 5042.5 Å, 5544.6 Å, and 5608.8 Å) Pb(II) lines at 11 600 K, adjusted to an electron density of 10^{17} cm^{-3},

with the data having an estimated relative uncertainty of about 30%. Lakićević and Purić[8] measured Stark shifts of 4245.1 Å, 5544.6 Å, and 5608.8 Å Pb(II) spectral lines at 10 000–20 000 K. In 1992, Djeniže et al.[9] measured Stark HWHM and shifts of Pb(II) 2203.5 Å and 4386.4 Å spectral lines at two temperatures, 28 000 and 27 000 K, and densities of electrons, 1.90×10^{17} cm^{-3} and 1.62×10^{17} cm^{-3}, respectively, with the estimated accuracy > 30%; measured in a pulsed linear arc plasma discharge, the driving gas was SF6 at the pressure of 130 Pa. Stark half-widths and shifts measured (within ± 15%) for three spectral lines of Pb(II) (4248.3 Å, 5545.7 Å, and 5610.4 Å, all wavelengths in vacuum) were obtained at two different values of the electron temperature and density by Puric et al.[10] Fishman et al.[11] determined experimental values for three visible lines (4388.1 Å, 4246.3 Å, and 6661.8 Å, wavelengths in vacuum) using an impulsive capillary light source and confirmed the values obtained by these authors in earlier work.[12] In Colón and Alonso-Medina,[13] the laser-induced lead plasma emission is used as light source to determine experimental Stark width of 31 Pb(II) spectral lines in the range of 1900–7000 Å.

Theoretical calculations of the profile, widths and shifts, of several spectral lines of Pb(II) have been carried out by other authors.[14–18] Lakićević[14] estimated the Stark half-widths for the 1681.7 Å resonant line of Pb(II) from systematic trends of Stark parameters versus inverse value of the lower level ionization potential. Semi-empirical values for the 5545.7 and 5610.4 Å lines wavelengths using the Coulomb approximation were also presented in this work. Djeniže et al.[15] calculated Stark HWHM values for 5042.5 Å, 5608.8 Å, and 6790.8 Å for 10^{17} cm^{-3} electron density and given electron temperature of 5000–40 000 K. Semi-empirical calculations of Stark widths for 43 lines of Pb(II) arising from ns $^2S_{1/2}$, np $^2P_{1/2,3/2}$, $^2D_{3/2,5/2}$, and 5f $^2F_{5/2,7/2}$ levels of Pb(II) were performed in works by Colón and Alonso-Medina[16,17] where Stark widths were presented as functions of temperature for an electron density of 10^{17} cm^{-3}. Recently, Blagojevic and Konjevic[18] performed semi-empirical calculations of Stark widths and shifts for the 4386.4 Å for 10^{17} cm^{-3} and given electron temperature of 11 300–27 000 K.

Laser-induced breakdown spectroscopy, also named laser-induced plasma (LIP) spectroscopy, is a simple technique because of its straightforward experimental setup. The characteristics of LIP depend upon several parameters characterizing: the features of the sample; properties of the ambient medium; laser wavelength and pulse duration; etc.[19–21] Laser-induced plasma, being an expanding plasma, changes its parameters rapidly during its evolution. The precise knowledge of the electron density, N_e, and the electron temperature, T_e, is a necessary requirement for the understanding of plasma processes. T_e and N_e are diagnostic indicators because from these two parameters one can predict the existing thermodynamic equilibrium in this plasma. Laser-induced plasma has been used with increasing frequency as spectroscopic sources for the measurement of Stark widths, see the example[13] published by this author. The Stark width and shift are dependent on the external electric field and, thus, of ions and electron densities, being required for deduce these parameters (N_e and T_e).

In the present work, the lead LIP emission is used as light source to determine experimental the Stark width and shift of two intense Pb(II) lines (2203.5 Å and 4386.5 Å) that occur at different times after the laser pulse, and in a different atmosphere (in vacuum and in argon atmosphere at different pressures), using parameters that have only been measured by Djeniže et al.[9] and Fishman et al.[11] as already mentioned above.

It is therefore the primary objective of this work to provide more accurate values for these parameters. This study was carried out and motivated by the verification of how these parameters are affected by the atmospheric conditions in which the plasma is generated. In this work, the evolution of the plasma was studied by an acquisition spectrum at several delay times after the laser pulse (0.15–9 μs), by measuring the density and temperature for each plasma obtained at each delay time and in different ambient conditions, in a vacuum and in the argon-controlled atmospheric conditions.

Here the Stark width and shift of line 2203.5 Å and line 4386.5 Å of Pb(II) in the electron number density range $(3 \times 10^{15}$–$1.3 \times 10^{17})$ cm^{-3} and electron temperature interval (8000–28 200) K, as well as graphs with the dependence of said parameters with the plasma parameters (temperature and electron density) are reported. In addition, the stability and homogeneity of electron density and temperature in the plasma are determined by means of a study of the temporal evolution in different environmental conditions. The local thermodynamic equilibrium (LTE) assumption has been discussed.

Experimental Setup and Measurement Details

The experimental setup applied in this work is similar to the LIP system used in previous papers, see Colon and Alonso-Medina[13] and others,[22–29] so only a brief description with an emphasis on new features is given here. The schematic diagram of the experimental system is shown in Fig. 1 of the mentioned references.[13,22,25,27]

The system consists of a Q-switched laser neodymium-doped yttrium aluminum garnet (Nd:YAG, Quantel YG585) laser with a 1064 nm wavelength, pulse energy of 290 mJ, pulse width of 7 ns, and a repetition rate of 20 Hz, and 1 m Czerny–Turner spectrometer, range 1900–7000 Å, with a 2400 grooves/mm holographic grating and a 50 μm external slit, equipped with a gated optical multichannel analyzer (OMA III EG&G PARC), which allowed the detection of each spectrum and its digital recording for later numerical

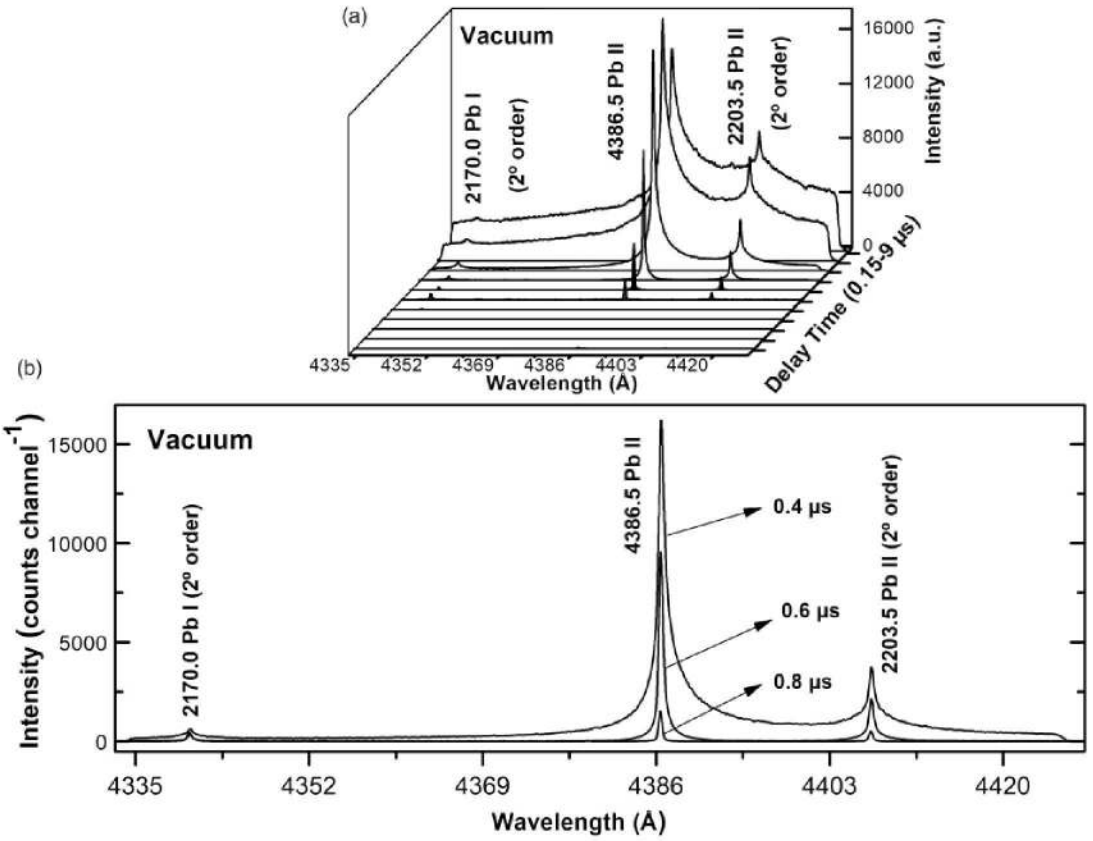

Figure 1. (a) Typical temporal distribution of a fragment of lead plasma-induced laser spectra in the region 4335–4425 Å at different time delays (0.15 μs, 0.2 μs, 0.3 μs, 0.4 μs, 0.6 μs, 0.8 μs, 1.5 μs, 2.5 μs, 4.5 μs, 6.5 μs, and 9 μs); and (b) the spectrum in detail in a vacuum at time delays (0.4 μs, 0.6 μs, and 0.8 μs).

analysis. The computer has a card used for communications, through which the communication is made with the central unit OMA. The whole process of acquisition data from the OMA has been programmed from this computer and the spectrum has been received, after the end throughout the measurement process. It has a time resolution with a minimum duration time window of 100–200 ns; the spectral band detected by the device is about 100 Å. This system allowed recording of spectral regions at different delays after the laser pulse and during a selected time interval.

The laser light was focused at a right angle onto the sample with a 12 cm focal length lens. In this work, a lead target (99.999% purity) was used. The laser irradiance on the blank was 2×10^{10} W cm^{-2}. The energy of the laser beam was checked with a power monitor, while the laser was firing at 20 Hz. A chamber was readied to generate the plasma with the target in a vacuum ($\approx 10^{-5}$ Torr) and in a controlled gas atmosphere. In a vacuum, the Pb(I), Pb(II), and Pb(III) spectral lines were recorded and in the argon atmosphere several spectral lines of the Ar(II) also appeared. The temperature, electron number density, and time evolution of laser-produced plasma can be controlled. The target was located inside the chamber, on top of a device capable of moving it horizontally with respect to the laser beam, focused in such a way that the plasma was formed in each measurement on the smooth surface of the target and not on the crater formed during the previous measurement. This could influence the intensity of the spectral lines and could lead to the destruction of the sample. This chamber features a quartz window that lets through light that is sent to the spectrometer entrance slit, located 8 cm from the plasma. Therefore, the radiation emitted by the plasma is collected directly by the entrance slit of the spectrometer. The temperature, electron number density, and time evolution of laser-produced plasma can be controlled.

The measurements consist in the accumulation of 20 laser pulses at a delay time, which were obtained after ablatively cleaning the target for two laser pulses in order to remove impurities. The spot size, measured at the target surface, was a circle with a diameter of 0.5 mm. The spectral lines have been obtained in the wavelength range of 2000–7000 Å. The relative spectral response of the experimental system in this range has been determined by using a calibrated deuterium lamp (range 2000–4000 Å) and a calibrated quartz–tungsten lamp (range 3500–7000 Å) with the same experimental conditions that were used in the

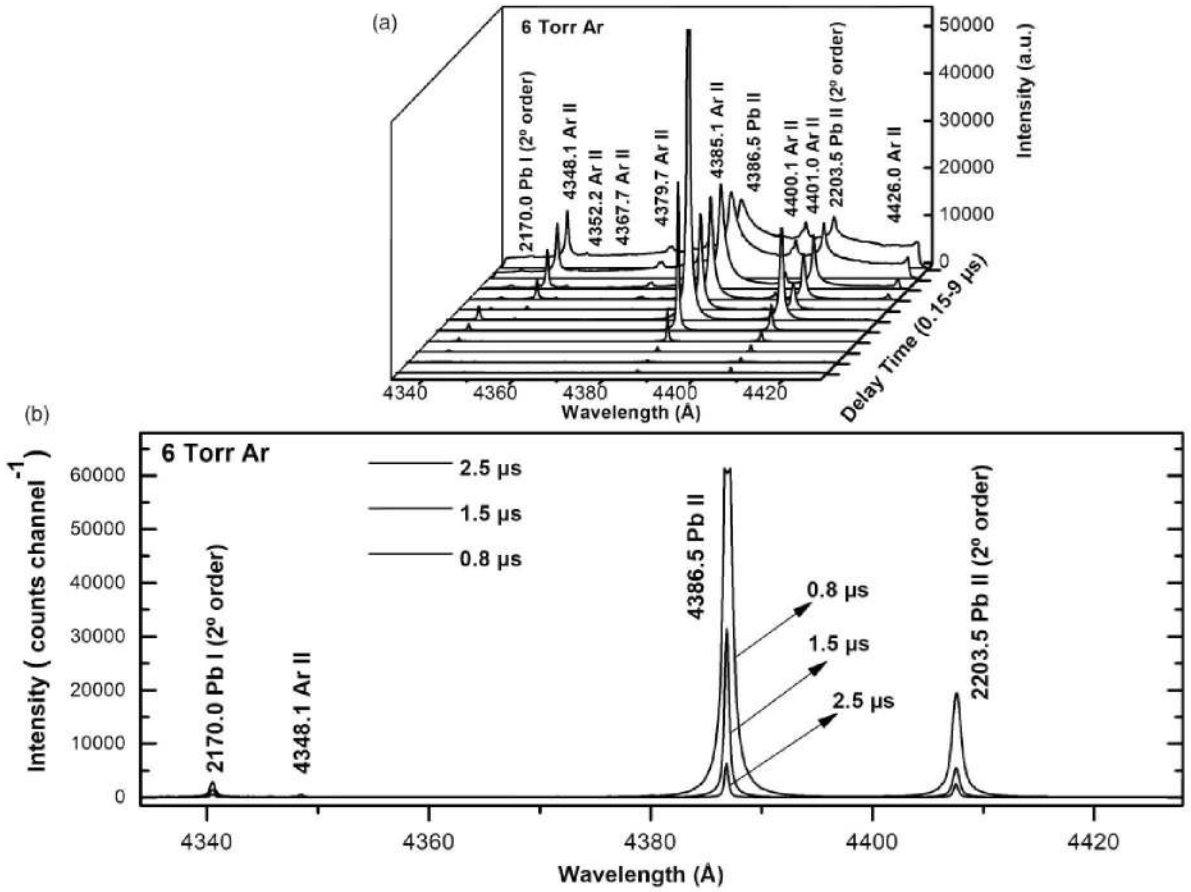

Figure 2. (a) Typical temporal distribution of a fragment of lead plasma-induced laser spectra in the region 4335–4425 Å at different time delays (0.15 µs, 0.2 µs, 0.3 µs, 0.4 µs, 0.6 µs, 0.8 µs, 1.5 µs, 2.5 µs, 4.5 µs, 6.5 µs, and 9 µs); and (b) the spectrum in detail in an argon atmosphere at 6 Torr (~800 Pa) at time delays (0.8 µs, 1.5 µs, and 2.5 µs).

measurements, reaching the maximum efficiency of the system in the range 3500–4500 Å (system sensitivity at 2200 Å is 3% and at 4386 Å is 60%). The estimated error of this measurement was about 5%. More details about the calibration of the system can also be found in previous studies.[13,22–26]

The temporal history of the plasma is obtained by recording the emission features at predetermined delays and at a fixed gate width. The measurements were repeated at several time delays (0.15–9 µs, delay from the laser pulse) and at a fixed gate time of 100 ns. For example, some spectra recorded at vacuum and at 6 Torr = 799.932 Pa of argon can be seen in Figs. 1 and 2.

The analysis of the spectra was made by fitting the observed line and shapes to numerically generated Voigt profiles and, with them, deconvoluting them to obtain the Lorentzian and Gaussian profiles; the instrumental profile is convoluted into the resulting profile. The instrumental profile needed for the numerical analysis of each spectrum was determined from the observation of several narrow spectral lines emitted by a hollow cathode lamp. This instrumental profile ($\Delta\lambda_{instrment}$) was Voigt profile full width half-maximum (FWHM) = 0.30 Å, Gaussian FWHM = 0.19 Å, and Lorentzian FWHM = 0.15 Å for a wavelength of 4380 Å; the estimated error of this measurement was about 3%. The distance for which two lines can be distinguished is 0.36 Å to the first order and 0.18 Å to the second order for this spectral range. Each spectrum is the average of five spectra at five different positions on the sample; few differences were observed between the five collected spectra, so an error of 5% for typical LIBS experiments is considered.

To fit the emission line profiles in the analysis and obtain relative intensity and the FWHM, a software tool has been used that is able to numerically generate Voigt profiles, convolution of the Lorentzian profile from the Stark broadening with the Gaussian profile from Doppler, and instrumental broadening by an analytical function. For the diagnostic of the plasma, the area under each line profile from the aforementioned fitting represents the relative intensity. The line intensities were obtained by subtracting the background intensity. The investigated spectral lines,

in this work, were well isolated from other spectral lines emitted by this plasma. We have obtained a good reproducibility ($\approx$3%) of the investigated spectral line radiation intensities.

To study the homogeneity of the plasma, the same experimental system was used, but in order to have spatial resolution, the light was focused by means of a lens on a 1 mm light guide being able to select the point of the plasma from which the light emission was observed. The lens and optical fiber connector have been mounted on a telescopic spring that allows one to vary their relative distance to coincide with the focus distance of the image of the plasma, keeping the plasma lens–optical fiber aligned. The support was mounted on an optical bench, allowing movement horizontally and vertically in a controlled manner, thereby varying the area of plasma whose image is detected in the optical fiber. More details about this procedure can be found in the references.[23,26] Local profiles were obtained after Abel inversion of the integrated intensity.[30]

The high density of particles forming the plasma is not always an advantage, because if transitions are studied whose lower level has a high population density, the spectral lines observed may have self-absorption. The self-absorption leads to a reduction of the line intensities, also causes asymmetries in the line shape, being able to produce an impediment to the adjustment of the line shape. Therefore, it is a priority to verify whether in line the self-absorption is present. Estimation of the absorption coefficient of all the lines studied will be shown in a later discussion.

Results and Discussion

Plasma Emission and Spectral Line Analysis

In the present work, the LIP emission spectrum was recorded in a vacuum and in an argon atmosphere for different time delays. The LIP lifetime mainly depends on the type of the surrounding ambient condition. The nature of LIP depends greatly on background gas conditions. The ambient surroundings are a significant factor affecting the ablation process and the properties of plasma. In addition, it was noticed that was only detected in some spectral lines emitted by said plasma and, that in some time delay, are self-absorbed. These changes are displayed by different spectroscopic peculiarities. For each spectral interval considered and at each instant of the plasma life, the optical emission was detected and analyzed.

By analyzing the spectrum, we can see that at the early stages of plasma evolution (first nanoseconds after the laser pulse, $<$ 100 ns), the continuum emission that dominates over lines emission is high due to mechanisms involving free electrons, inverse Bremsstrahlung, radiative recombination, and photoionization. An adiabatic expansion of the plasma plume occurs after termination of the laser pulse, this is a conversion of thermal energy into kinetic energy of elements in the plasma. So, we cannot obtain accurate information about atoms and ions because of the overwhelming continuum emission for short delay times ($\approx$ 150–200 ns). At these early times, the electron density is very high and spectral lines of the different species are broadened by the Stark effect due to the electron collisions. At the longer times of the plasma expansion, the spectral lines become narrower, indicating a decrease of electron density. The temperature decreases rapidly with plasma expansion. The peak widths and profiles in lines spectra are primarily dictated by the temperature and electron density of plasma. As we have already mentioned above, in order to extract useful spectroscopic information from such plasma, one needs to understand how the shapes of spectral lines evolve with time in the different ambient conditions. In this work, the measurements were repeated at several time delays from the laser pulse, 0.15–9 μs. The electron density and electron temperature have been measured at different time delays and at different ambient conditions: in vacuum and in an argon atmosphere at different pressures, 6 Torr ($\sim$800 Pa), 12 Torr ($\sim$1600 Pa), 24 Torr ($\sim$3200 Pa), ambient conditions where the plasma is generated. The pressure of the ambient atmosphere is one factor of the controlling parameters of the plasma characteristic.

Figures 1 and 2 give an overview of the plasma evolution in media of different of aggregation and pressure. Figure 1 shows the emission spectrum of lead plasma, in a vacuum, covering the spectral region of 4335–4425 Å, the same region collected in the previous work.[13] Figure 1a shows the spectra obtained at 11 different time delays (0.15 μs, 0.2 μs, 0.3 μs, 0.4 μs, 0.6 μs, 0.8 μs, 1.5 μs, 2.5 μs, 4.5 μs, 6.5 μs, and 9 μs). A spectral line Pb(I) (in the second order), the line resonant 2170.0 Å ($5d^{10}6s^2$ 6p ($^2P_{1/2}$) 6d $^3D_1 \rightarrow 5d^{10}6s^26p^2\ ^3P_0$, in the second order), and two spectral lines of Pb(II), line 4386.5 Å ($5d^{10}6s^2$ (^1S) 5f $^2F_{5/2} \rightarrow 5d^{10}6s^2$ (^1S) 6d $^2D_{3/2}$), and line 2203.5 Å ($5d^{10}6s^2$ (^1S) 7s $^2S_{1/2} \rightarrow 5d^{10}6s^2$ (^1S) 6p $^2P_{3/2}$, in the second order), superposed on the continuous signal, are observed. A short time delay (0.15 μs, 0.2 μs, 0.3 μs, and 0.4 μs) shows that these lines are deformed and have low symmetry and strong broadening. The continuous signal weakens quickly as the plasma gets colder; on the contrary, the peaks of the lines persist for longer times. Figure 1b shows the spectrum in three different time delays of 0.4 μs, 0.6 μs, and 0.8 μs in detail, where from the time delay at 0.6 μs these lines already have a symmetrical shape and better S/N ratio.

Based on Fig. 1, it is evident that the continuous emission dominates the early stages of the formation of the plasma, that the plasma expansion in a vacuum is very fast, thus causing the plasma density to drop to values in the order of 10^{15} cm^{-3}, as we will see later. In addition, it is evident that a lower electron density implies limited Stark broadening and radiative recombination, which renders

spectral lines optically thin and resolves the continuum greatly. In the experimental conditions described in this paper, the plasma generated evolves expanding and cooling via a de-excitation and recombination process; it becomes extinct in times in the range of 1.5–6.5 μs, returning again with little intensity to 9 μs.

It should be noted that to decrease the effect of the continuous radiation, it is necessary to delay the acquisition of the spectrum compared to the impulse of an appropriate time interval laser. It should also be noted that in a vacuum, plasma evolution is fast and LTE is easier to obtain in the final stages of evolution than in the early stages.[26,29] The use of emission spectroscopy for the measurement of temperature and electron density of the plasma requires optical thin spectral lines.

Figure 2 shows the emission spectrum of lead plasma covering the spectral region of 4335–4425 Å in a controlled argon atmosphere at 6 Torr.[13] Figure 2a shows the spectra obtained at 11 different time delays (0.15 μs, 0.2 μs, 0.3 μs, 0.4 μs, 0.6 μs, 0.8 μs, 1.5 μs, 2.5 μs, 4.5 μs, 6.5 μs, and 9 μs). A spectral line Pb(I) (in the second order), the line resonant 2170.0 Å, and two spectral lines of Pb(II), line 4386.5 Å and line 2203.5 Å (in the second order), superposed on the continuous signal, are observed. In the early time delays, 11 spectral lines of Ar(II) are also observed (lines 4331.2 Å, 4348.1 Å, 4352.2 Å, 4367.7 Å, 4370.7 Å, 4371.3 Å, 4379.7 Å, 4385.1 Å, 4400.1 Å, 4401.0 Å, and 4426.0 Å), based on the data listed in the tables from National Institute of Standards (NIST),[31] superposed on the continuum and disappeared to time delays > 0.7 μs, except for the most intense lines (see 4348.1 Å) that last up to the delay time of 4.5 μs to reappear at 9 μs. The atomic and ion lines of Pb are mainly emitted from the hot plasma core, the ion lines of Ar originate from the cold plasma periphery. In 9 μs from the laser pulse or the colder zone of the LIP, new processes involving heavy particles collisions should be considered. It is also noticed that due to confinement produced by gas, the lines of Pb(I) and Pb(II) are growing in intensity, reaching their maximum value at the delay time 0.8 μs, and that these lines remain up to delay time 9 μs, but with a very low

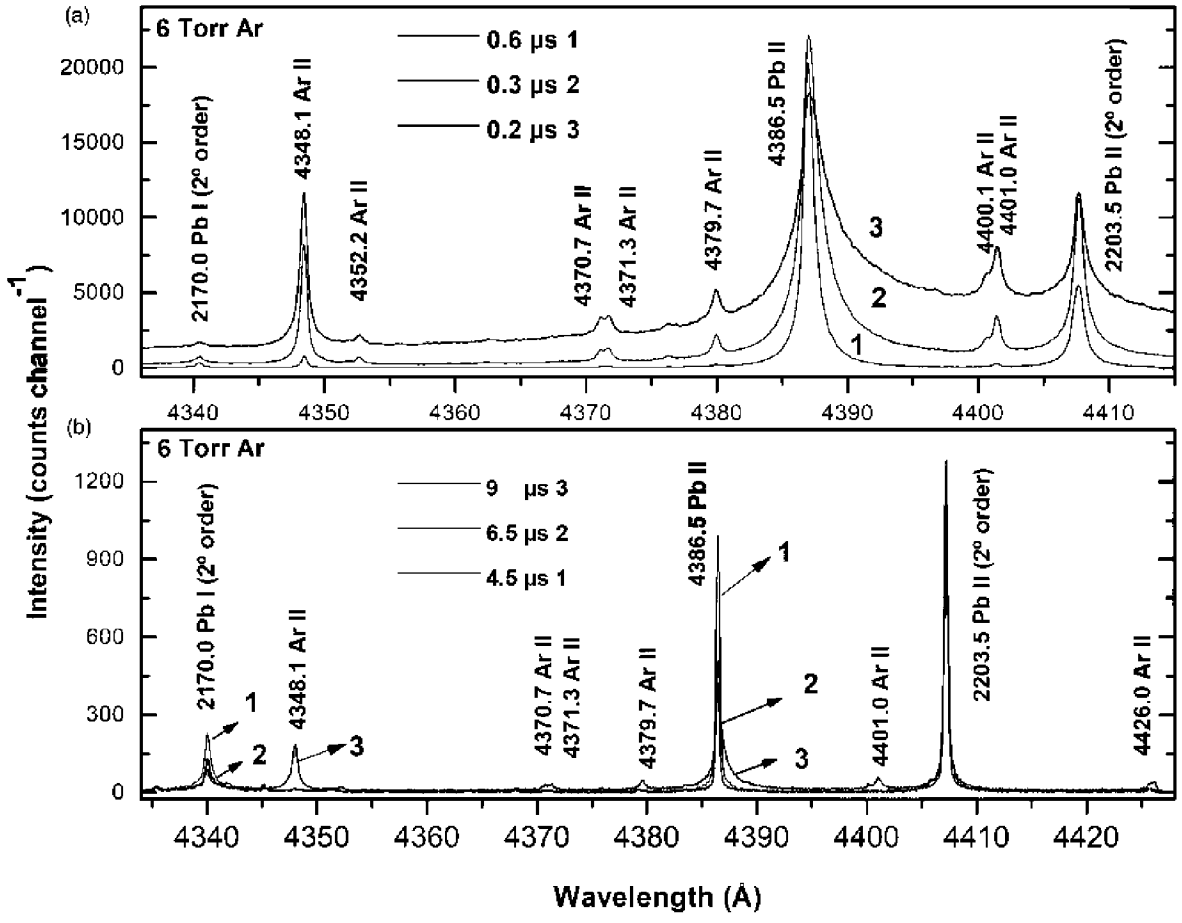

Figure 3. (a) Typical temporal distribution of a fragment of lead plasma-induced laser spectra in the region 4335–4425 Å at different time delays (0.2 μs, 0.3 μs, and 0.6 μs); and (b) details of the spectrum in an argon atmosphere at 6 Torr (~800 Pa) at time delays (4.5 μs, 6.5 μs, and 9 μs).

intensity (< 300 counts channel^{-1} the line resonant 2170.0 Å, in the second order, of Pb(I) and 1200 counts channel^{-1} the line resonant 2203.5 Å (second order) of Pb(II). Figure 2b shows the spectrum in three different time delays (0.8 μs, 1.5 μs, and 2.5 μs) in detail, where from the time delay at 0.8 μs self-reversal is evident in the spectral line 4386.5 Å of Pb(II). The temporal distributions of plasma intensity allow us to see that higher degree of plasma confinement experienced in the argon atmosphere than in vacuum, Fig. 2a.

More details in Fig. 3 show the plasma spectra obtained at three different time delays (0.2 μs, 0.3 μs, and 0.6 μs) in a controlled argon atmosphere at 6 Torr, where it is observed in detail that at time delay 0.6 μs the lines of Ar(II) still appear, but with a low intensity, and also that the lines 4386.5 Å and 2203.5 Å (second order) of Pb(II), as discussed above, appear deformed, have low symmetry, and are very wide in the time delays 0.2 μs and 0.3 μs. In general, the presence of the argon atmosphere at 6 Torr tends to improve spectra by increasing the intensity or S/N ratio and improving the resolution. This is because the ambient argon atmosphere impedes the expansion of the plasma, which could cause an increase in both emission lifetime and emission intensity. Figure 3b shows the plasma spectra obtained at three different time delays (4.5 μs, 6.5 μs, and 9 μs); the line 4348.1 Å of Ar(II) disappears at time delays $\approx$4.5–6.5 μs to reappear at 9 μs, with very little intensity.

It is known that the spectroscopic study of shapes and shifts of spectral lines is usually a difficult task due to absorption effects that may cause difficulties in unmasking the true line profiles. The absorption will have the effect of distorting and broadening of lines, although it is also known that self-absorption only slightly distorts the shape of a dispersion profile. When plasma has a strong gradient between the center and the periphery, rays issued from the center can be reabsorbed by the colder species located in the periphery. This translates into a decrease in the intensity of the line and transforming its profile. The high density of particles forming the plasma is not always an advantage, because if transitions are studied whose lower level has a high population density observed lines can present self-absorption. If the self-absorption originates mostly from the cooler boundary layer of much lower electron density and if the spectral resolution is sufficient, the line center exhibits readily recognizable self-reversal.

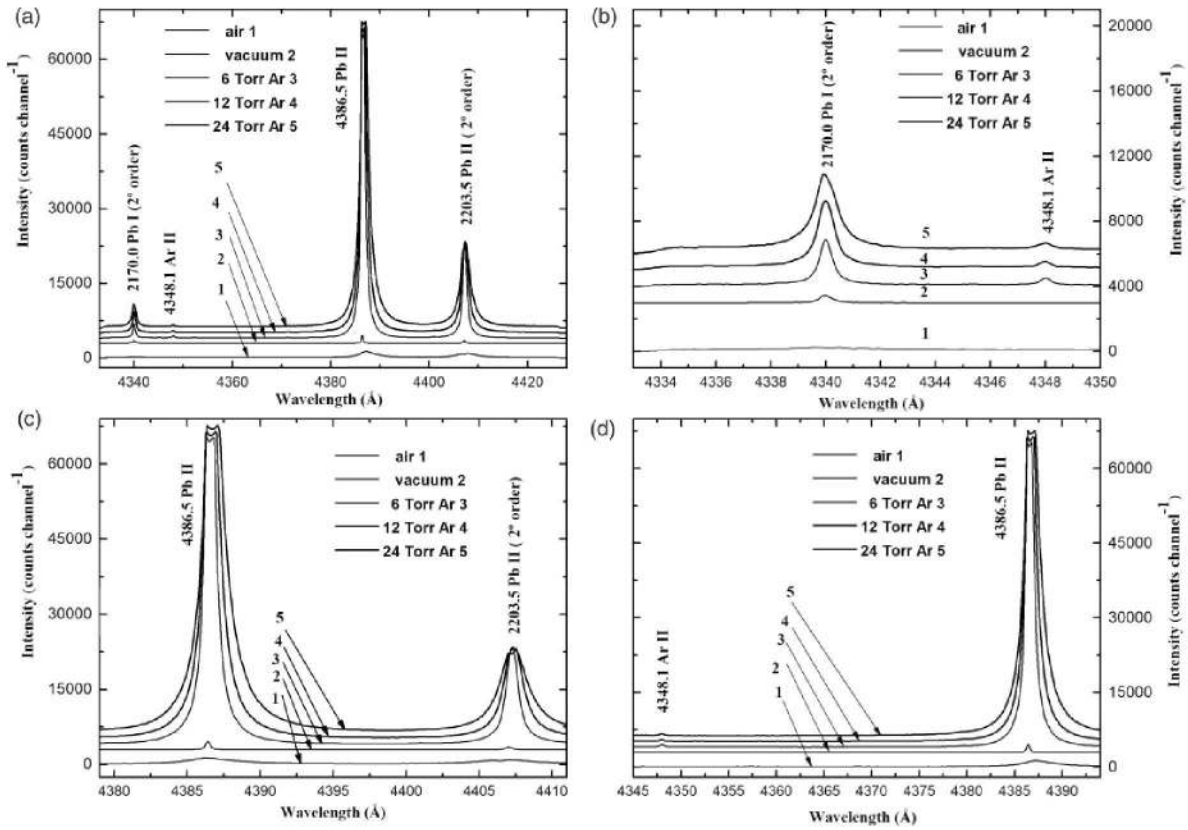

Figure 4. (a) Typical spectrum in the region 4334–4425 Å recorded at a time delay of 0.8 μs and different ambient conditions; (b) the resolved part of the short wavelength 4334–4350 Å region; (c) the resolved part of the short wavelength 4380–4410 Å region; and (d) the resolved part of the short wavelength 4345–4390 Å region.

In addition, it was only detected in some spectral lines emitted by said plasma, and in some instances of its lifetime is self-absorbed (see Figure 4a–d). Figure 4 shows the emission spectrum of lead plasma covering the spectral region 4335–4425 Å and in different ambient conditions: in a vacuum; in air at atmospheric pressure; and in an argon atmosphere at different pressures (6 Torr, 12 Torr, 24 Torr), and at a time delay of 0.8 μs. The Ar(II) line at 4348.1 Å, as already mentioned, remains very intense. The Pb(II) lines at 4386.5 Å and 2203.5 Å (second order) showed signs of self-absorption. Line 4386.5 Å showed self-reversal in the argon atmosphere at different pressures (6 Torr, 12 Torr, 24 Torr) and line 2203.5 Å (second order) in 24 Torr; there is also a slight shift in the location of the center of the peaks, especially for air and argon compared to a vacuum. Figure 4b presents in detail the 2170.0 Å line in the second order of Pb(I) and line 4348.1 Å of Ar(II), giving the location of the center of the peaks maintained in the different ambient conditions. It is evident in Fig. 4c and 4d that the intensity of the line at 4386.5 Å Pb(II) under argon increases and widens with increasing pressure of argon; that is to say, the spatial confinement of plasma becomes stronger with an increase of the ambient conditions. In the case of these lines are the radiative transfer effects, among other reasons, which tend to widen them by self-absorption reaching a self-reversal. In addition, shift lines are observed, at the different time delays, of the red to blue, "redshift" defined as positive and "blueshift" as negative, which will be explained later.

Figure 5 shows the emission spectrum of lead plasma covering the spectral region 4335–4425 Å and in air at atmospheric pressure. Figure 5a shows the plasma spectra obtained at 11 different time delays (0.15 μs, 0.2 μs, 0.3 μs, 0.4 μs, 0.6 μs, 0.8 μs, 1.5 μs, 2.5 μs, 4.5 μs, 6.5 μs, and 9 μs). A spectral line of Pb(I) (the line resonant is 2170.0 Å, in the second order) and two spectral lines of Pb(II), line 4386.5 Å and line 2203.5 Å (in the second order), have been observed superposed on the continuous signal, and short

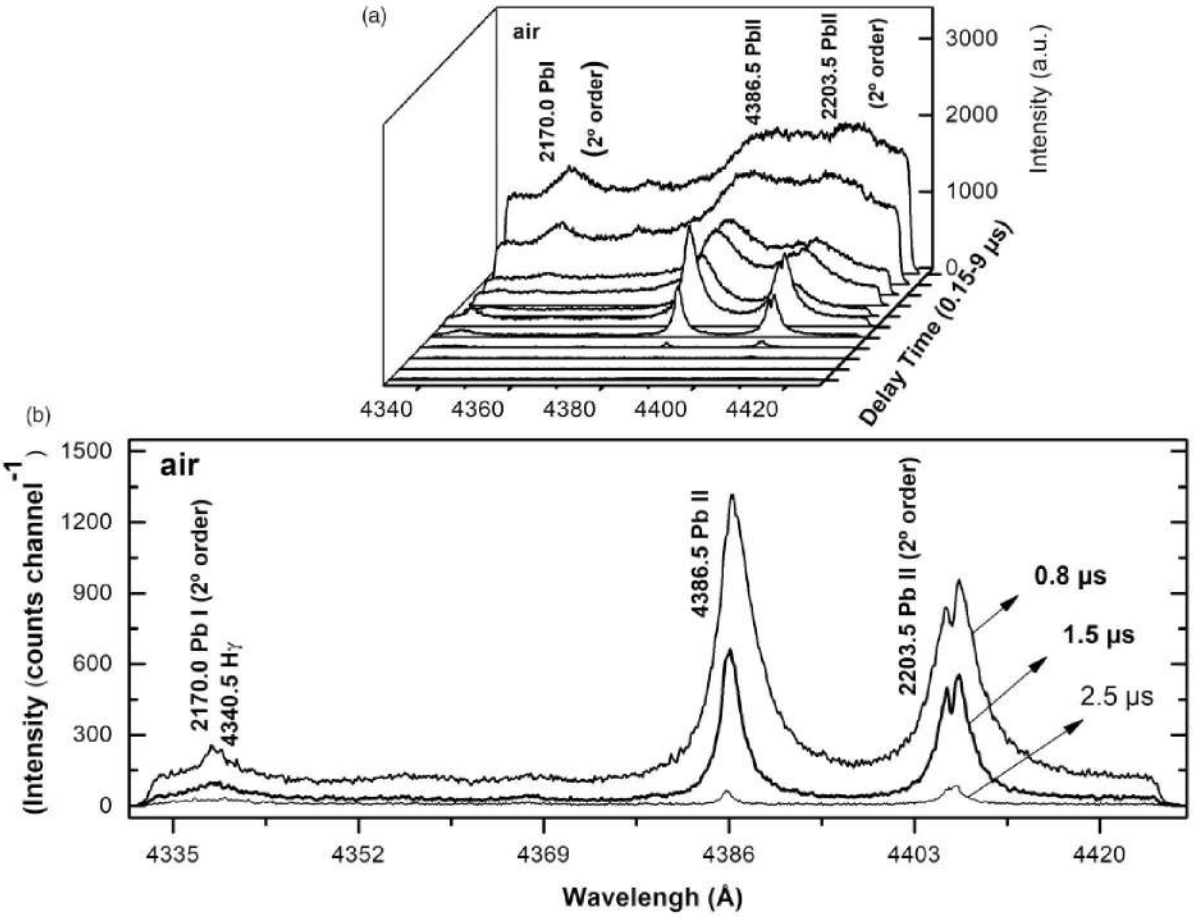

Figure 5. (a) Typical temporal distribution of a fragment of lead plasma-induced laser spectra in the region 4335–4425 Å at different time delays (0.15 μs, 0.2 μs, 0.3 μs, 0.4 μs, 0.6 μs, 0.8 μs, 1.5 μs, 2.5 μs, 4.5 μs, 6.5 μs, and 9 μs); and (b) detail of the spectrum in air at atmospheric pressure at time delays (0.8 μs, 1.5 μs, 2.5 and μs).

time delays of 0.8–2.5 μs have been observed with strong broadening and asymmetries in line shapes and self-absorption in these lines. In addition, the line Hγ 4340.5 Å can be mixed with the line 2170.0 (second order) of Pb(I). The presence of self-absorption in lines adversely affects both the peak intensity as well as resolution. Indeed, a self-absorbed emission line has a profile collapsed with a crash sometimes almost total peak or a digging more or less deep in the center of line. When the phenomenon is very intense, it will produce a self-reversed peak, as seen in Fig. 5b. Self-absorption has been observed in the resonance lines of Pb(I) and Pb(II). A self-reversed peak is evident in the spectral line 2203.5 Å (second order) of Pb(II). The peak is first flattened and then reversed following a dip in the middle of the line; neglect of this self-absorption effect can be critical. Observation of a self-reversal dip at the top of the line is a special case, which is a clear sign of strongly inhomogeneous plasma. In this work, the use of multiple pulses (accumulation of 20 laser pulses) induces deep modifications in the plasma dynamics and, consequently, in the emission spectra at time delay 0.8 μs, as seen in Figs. 4 and 5. The lead plasma obtained would not be a good spectroscopic source. In the present study, the sample does not contain any hydrogen, hence the only source of hydrogen is air (~0.005%). For all this, in atmosphere air at atmospheric pressure not performed this study.

Determination of the Plasma Temperatures and the Electron Number Densities: Temporal Evolution

The temperature (T) and the electron number density (N_e) are very important parameters for plasma and their knowledge is useful for their characterization. It is well known that in order to give a correct interpretation of the emission spectrum, it is necessary to know the thermodynamic state of the plasma. The classical approach to the study of LIP spectroscopy is based on the assumption that temperatures define the distributions of kinetic energy, excitation energy, and ionization energy are considered equal with LTE. Once formed, the plasma is usually assumed to reach a situation of LTE, i.e., the population density of the atomic and ionic electronic states is described by the Boltzmann distribution.[32,33] The intensity of the emission lines of the plasmas obtained, in fact, is strictly correlated with the population distribution among the atomic energy levels and among the ionization stages. The plasma temperature was measured using the Boltzmann plot method for determining the excitation temperature and Saha equation for determining the N_e, and it is well known that LTE plasma is characterized by single temperature.[32–36] Cristoforetti et al.[35,36] have conducted a detailed study. The temperature and electron number density of plasmas formed in vacuum and in argon atmosphere at different pressures (6, 12, and 24 Torr) have been determined at each time delay elapsed from the laser pulse (in particular 0.3–6.5 μs).

It is well known that in emission spectroscopy, to measure both temperature and electron density requires optically thin spectra lines, that is to say, for extracting quantitative data from the line intensities, it is important to verify that the plasma is optically thin. Self-absorption has traditionally been one of the main sources of error in the measurement of intensities of the spectral lines and has a great influence on the values of the transition probabilities and of Stark parameters. In this work, we have verified that the spectral lines used to obtain the parameters of the plasma under study (N_e and T_e) do not present absorbed.

A variety of techniques exists to determine the presence of self-absorption effects, which are convenient for LIP application: (1) the technique of doubling optical path through plasma by means of concave mirror employed by Moon et al.,[37] correction procedure highly sensitive; (2) the method of checking line intensity ratios within multiplets that are expected to adhere to LS coupling employed by Radziemski et al.[38] (this technique can be used only as an indicator of whether self-absorption can be applied for measurement of absorption coefficient); and (3) a modification of this technique is the "curve of growth" method described in Gornushkin et al.[39] (varying concentration of the studied sample and observe variations of line intensity ratio within multiplets).

In this work, the absence of self-absorption has been checked using a method described by Thorne.[40] The degree of self-absorption can be explained by the self-absorption coefficient (k_ω). With the obtained values of N_e and T we can calculate the absorption coefficient (k_ω) for the studied lines, using the following equation, expressed in m^{-1}:[30,40]

$$k_\omega = \frac{\pi e^2}{2\varepsilon_0 mc} f_{ik} N_i \left[1 - \frac{N_k g_i}{N_i g_k}\right] g(\omega) \quad (1)$$

where e and m are the charge and the mass electron, respectively, c is the speed of light, f_{ik} is the oscillator strength (absorption), and N_k and N_i are the population densities of the lower-level energy and the upper-level energy, respectively, estimated at approximately equal to the electron density, this being an upper limit, g_i and g_j are the statistical weight of state, and $g(\omega)$ is the normalized profile of the line. In the maximum, $\omega = 0$, and for a Lorentz profile, $g(o) = 2/\pi\Gamma$, where Γ is the FWHM of the line. A line may be considered optically thin if k_ω (cm^{-1}) $\times D$ (cm) < 1;[33] in the present work, $D \approx 1$ mm, the value of the optical depth $k_\omega D$ is not > 0.1. For all this, in atmosphere air at atmospheric pressure not performed this study: both in a vacuum and in argon at 6 Torr and 12 Torr, with the exception of the lines (lines 4386.5 Å and 2203.5 Å [in the second order] of Pb(II)) in the study that in

the delay 0.8 μs suffers self-reversal, in atmosphere of argon (see Fig. 4). For example, line 4386 of Pb(II) at time delay 0.4 μs: (1) in vacuum, $k_\omega D = 0.02$; (2) in 6 Torr argon atmosphere, $k_\omega D = 0.04$; (3) in 12 Torr argon atmosphere, $k_\omega D = 0.06$; and (4) in 24 Torr argon atmosphere, $k_\omega D = 0.1$. In the argon atmosphere to 24 Torr, in the first time delays (0.15–0.7 μs), some lines obtained a value of $k_\omega D > 0.6$, e.g., at time delay 0.2 μs for the line 3639.57 of Pb(I), $k_\omega D = 0.7$. This line is one that we will use to obtain the temperature, as will be seen later. We can conclude that for a plasma thickness of 1 mm, the experiments were carried out in optically thin lead plasma.

Determination of the Plasma Temperature

The excitation temperature was determined by constructing Boltzmann plots. As is well known, in optically thin the relative line intensities $\left(I_{ij}^{\lambda}\right)$ of the lines emitted from a given state of excitation can be used to calculate the temperature, if the transition probabilities (A_{ij}) are known, by the expression:[32–34]

$$I_{ij}^{\lambda} = \frac{A_{ij} g_i}{U(T)} N \exp\left(\frac{-E_i}{kT}\right)$$
$$\ln\left(\frac{I_{ij}^{\lambda}}{A_{ij} g_i}\right) = \ln\left(\frac{N}{U(T)}\right) - \frac{E_i}{kT} \qquad (2)$$

for a transition from a higher state i to a lower state j, I_{ij}^{λ} is the integrated measured line intensity, in counts per second, A_{ij} is the transition probability, λ is the wavelength of the optical transition between two levels, E_i is the excited level energy, g_i is the energy and statistical weight of level i, $U(T)$ is the atomic species partition function, N is the total density of emitting atoms, k is the Boltzmann constant, and T is the temperature in K. If we were to plot $\ln(I_{ij}^{\lambda}/A_{ij}\, g_i)$ versus E_i, for lines of known transition probability (Boltzmann plot), the resulting straight line would have a slope $-1/kT$, and therefore the temperature could be obtained without having to know the total density of atoms or the atomic species partition function. For this purpose, the total intensity (area) must be determined for each spectral line. In this work, various transitions have been carefully chosen.

The temperature has been estimated, in each ambient condition and in each delay time, by using spectral lines of Pb(I), Pb(II), Pb(III), and Ar(II) (Table 1), as it is better to use transitions involving upper level states which lie close to the ionization energy level. In a vacuum, the spectral lines 3854.08 Å, 3689.31 Å, 3729.69 Å, and 3655.50 Å of Pb(III) have been used at short time delays (0.3 μs, 0.4 μs) and the spectral lines 3683.46 Å, 3639.57 Å, 3739.99 Å, and 3572.73 Å of Pb(I), the spectral lines 5608.90 Å, 4244.92 Å, 3785.99 Å, 3718.30 Å, and 3713.98 Å of Pb(II) have been used at long time delays (0.6 to 6.5 μs), e.g., a typical Boltzmann plot is shown in Fig. 6. In the argon atmosphere, the spectral lines 4401.0 Å, 4348.1 Å, 4379.7 Å, and 4370.7 Å of Ar(II) have been used at short time delays (0.3–0.6 μs), see Fig. 7. These estimated values of electron temperatures have been obtained from the relative line intensities measured in this work, required for applying this method, and the transition probabilities (A_{ij}) corresponding to these lines that have been taken from the bibliography[22,23,27,31,41] and are presented in Table 1. The spectral lines were selected according to the following criteria: (1) the overlapping of spectral lines must be avoided; (2) the emission intensity must be large enough to ensure the observation with a sufficiently large S/N intensity ratio; (3) that self-absorption does not appear; and (4) that the lines must have a weak enough optical thickness to have a significant correlation between elemental concentration and line intensity. The energies of the different levels are those of Moore[42] and the corresponding wavelengths are those of Lochte-Hotgreve and Richter[31] and Moore.[42]

As mentioned above, the electron temperature from the Boltzmann plot was determined from the line intensities of Pb(II) (5608.9 Å, 4244.92 Å, 3785.99 Å, 3718.30 Å, and 373.98 Å) obtained in the lead plasma produced for the laser of a vacuum and time delay 1.5 μs, 13 080 K for $\Delta E_i = 2.599$ eV (Fig. 6b) and the line intensities of Pb(III) (3854.08 Å, 3689.31 Å, 3729.69 Å, and 3655.50 Å) obtained in the lead plasma produced for the laser of argon at 6 Torr and delay time 0.4 μs, 20 600 K for $\Delta E_i = 5.16$ eV (Fig. 6a), all the data exhibited a linear fit with a correlation coefficient than 0.99927 and 0.99989, respectively. From the line intensities of Ar(II) (4401.0 Å, 4348.1 Å, 4379.7 Å, and 4370.7 Å) obtained in the lead plasma produced for the laser of argon at 6 Torr and time delay 0.3 μs, 24 150 K for $\Delta E_i = 2.27$ eV (Fig. 7), all the data exhibited a linear fit with a correlation coefficient than 0.99202 (Fig. 7). The relative uncertainty were estimated from the standard deviation of the slopes obtained in the least squares fittings; the uncertainties that are taken into account are: (1) the line profile fitting procedure (≈ 1%); (2) the integrated intensities of the spectral line determination in this work (≈ 3%); and (3) the transition probabilities (depending on each line), see Table 1.

To obtain the Stark width and shift of line 2203.5 Å and line 4386.5 Å of Pb(II) that are provided in this work, the LTE has been ensured in each plasma under study. For example, in an argon atmosphere at 6 Torr and with a time delay of 0.3 μs, the temperature obtained was: (1) 24 150 K with the lines of Ar(II) Table 1; (2) 26 500 K with the lines of Pb(III) (Table 1); and (3) 25 300 K with the lines of the Pb(II) (Table 1). These values do not ensure the same temperature[35,36] and LTE is not assured; therefore, Stark broadening has not been measured at this time delay.

As mentioned above, the temperature decreases rapidly with plasma expansion. The temporal evolution of the

Table I. Spectroscopic parameters of Pb I, Pb(II), Pb(III), and Ar(II) spectra lines using in the determination of the temperatures.

Specie	Transition	λ (Å)[a]	E_i (eV)[a]	A_{ij} ($\times 10^7$ s^{-1})
Pb(I)				
	$5d^{10}6s^26p\ (^2P_{1/2})\ 7s\ ^3P_0 \rightarrow 5d^{10}6p^2\ ^3P_1$	3683.46	4.334	16.76 ± 1.07[b]
	$5d^{10}6s^26p\ (^2P_{1/2})\ 7s\ ^3P_1 \rightarrow 5d^{10}6p^2\ ^3P_1$	3639.57	4.375	3.08 ± 0.21[b]
	$5d^{10}6s^26p\ (^2P_{1/2})\ 7s\ ^3P_2 \rightarrow 5d^{10}6p^2\ ^1D_2$	3739.99	5.974	5.33 ± 0.34[b]
	$5d^{10}6s^26p\ (^2P_{1/2})\ 7s\ ^1P_1 \rightarrow 5d^{10}6p^2\ ^1D_2$	3572.73	6.130	9.53 ± 0.60[b]
Pb(II)				
	$5d^{10}6s^2\ (^1S)\ 7p\ ^2P_{3/2} \rightarrow 5d^{10}6s^2\ (^1S)\ 7s\ ^2S_{1/2}$	5608.90	9.581	8.48 ± 0.85[c] 8.31 ± 0.83[d]
	$5d^{10}6s^2\ (^1S)\ 5f\ ^2F_{7/2} \rightarrow 5d^{10}6s^2\ (^1S)\ 6d\ ^2D_{5/2}$	4244.92	11.470	11.50 ± 1.16[c] 11.21 ± 1.66[d]
	$5d^{10}6s^2\ (^1S)\ 5f\ ^2F_{5/2} \rightarrow 5d^{10}6s^2\ (^1S)\ 6p^{24}P_{3/2}$	3785.99	11.472	1.01 ± 0.10[c] 0.96 ± 0.14[d]
	$5d^{10}6s^2\ (^1S)\ 9s\ ^2S_{1/2} \rightarrow 5d^{10}6s^2\ (^1S)\ 7p\ ^2P_{1/2}$	3718.30	12.565	1.20 ± 0.20[c] 1.75 ± 0.28[d]
	$5d^{10}6s^2\ (^1S)\ 8d\ ^2D_{5/2} \rightarrow 5d^{10}6s^2\ (^1S)\ 7p\ ^2P_{1/2}$	3713.98	12.918	4.19 ± 0.62[c]
Pb(III)				
	$5d^{10}6s\ (^2S)\ 7p\ ^3P_2 \rightarrow 5d^{10}6s\ (^2S)\ 7s\ ^3S_1$	3854.08	21.823	20.8 ± 2.1[e]
	$5d^{10}6s\ (^2S)\ 7p\ ^1P_1 \rightarrow 5d^{10}6s\ (^2S)\ 7s\ ^3S_1$	3689.31	21.967	7.0 ± 0.75[e]
	$5d^{10}6s\ (^2S)\ 8s\ ^3S_1 \rightarrow 5d^{10}6s\ (^2S)\ 7p\ ^3P_1$	3729.69	24.535	14.3 ± 1.5[e]
	$5d^{10}6s\ (^2S)\ 5g\ ^3G_3 \rightarrow 5d^{10}6s\ (^2S)\ 5f\ ^3F_2$	3655.50	26.983	27.5 ± 2.8[e]
Ar(II)				
	$3s^23p^4\ (^3P)\ 4p\ ^4P_{5/2} \rightarrow 3s^23p^4\ (^3P)\ 3d\ ^4D_{7/2}$	4401.00	19.222	3.04 ± 0.61[f]
	$3s^23p^4(^3P)4p^4D^0_{7/2} \rightarrow 3s^23p^4(^3P)4s^4P_{5/2}$	4348.10	19.494	11.71 ± 1.17[f]
	$3s^23p^4(^3P)4p^4D^0_{1/2} \rightarrow 3s^23p^4(^3P)4s^4P_{1/2}$	4379.70	19.642	10.00 ± 1.00[f]
	$3s^23p^4(^1D)4p^2D^0_{3/2} \rightarrow 3s^23p^4(^3P)3d^2D_{3/2}$	4370.70	21.492	6.60 ± 1.32[f]

[a]Moore.
[b]Alonso-Medina et al.
[c]Alonso-Medina.
[d]Alonso-Medina.
[e]Alonso-Medina.
[f]NIST.
E_i, excited level energy; A_{ij}, transition probability.

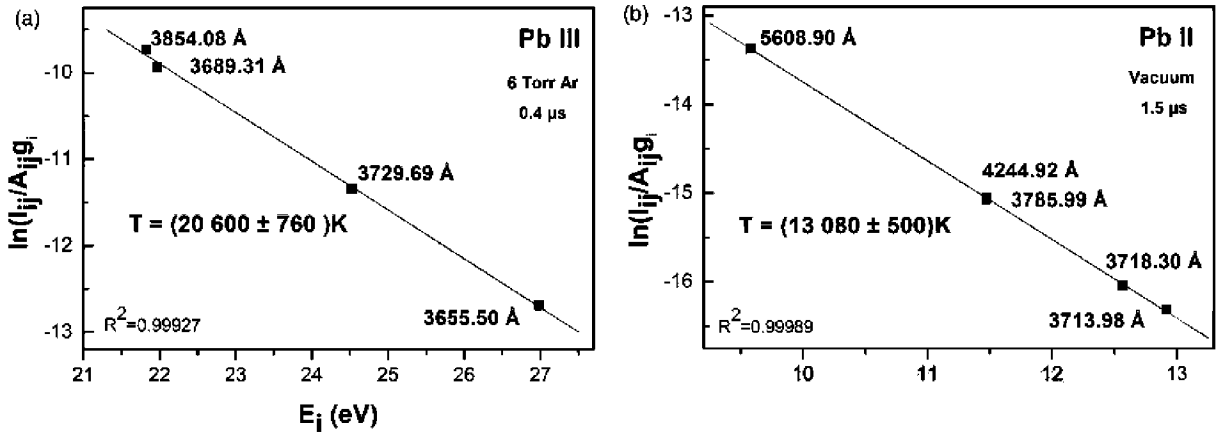

Figure 6. Boltzmann plot for temperatures certain of a laser-induced lead plasma obtained from two ambient conditions and two time delays: (a) for Pb(III), 6 Torr Ar, and 0.4 μs, and (b) for Pb(II), vacuum, and 1.5 μs.

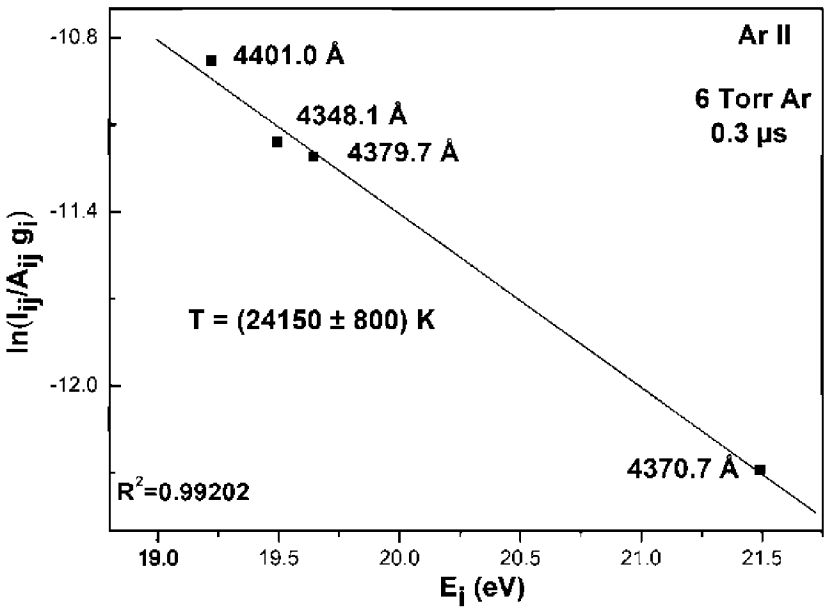

Figure 7. Boltzmann plot for temperatures certain of a laser-induced lead plasma obtained from 6 Torr Ar and time delay 0.3 μs.

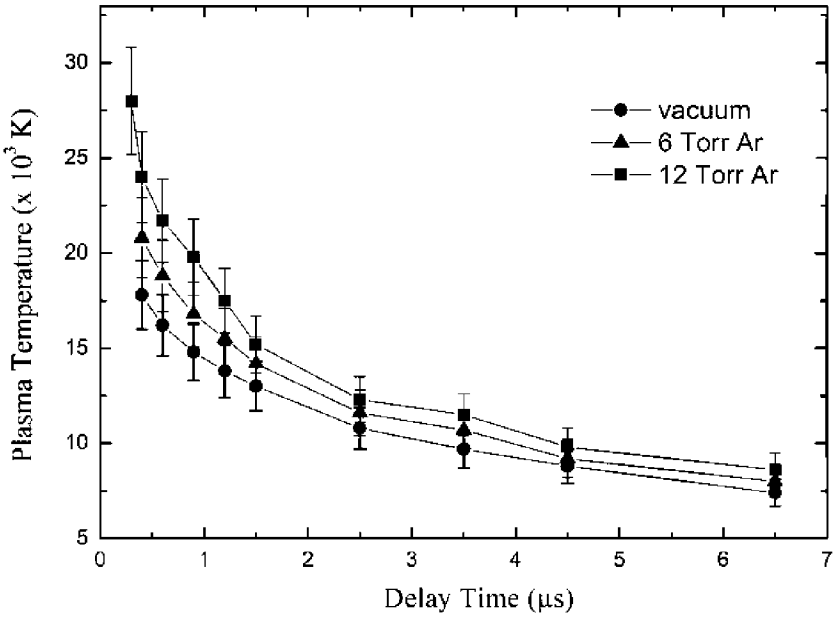

Figure 8. Temporal evolution of temperature, T_e, vs. time delays in various atmospheres: in a vacuum (circles), in 6 Torr Ar (triangles), and in 12 Torr Ar (squares).

plasma temperature in three different atmospheres (vacuum and argon at 6 Torr and 12 Torr) is shown in Fig. 8 and the temperature measurement error of about 10% is indicated by the vertical error bars. As can be seen, the plasma temperatures are high in the three atmospheres for the time delays (0.3–0.6 μs). This is accompanied by a decrease in the temperature from about 20 600 K to 8000 K in the atmosphere at argon 6 Torr pressure comparing with 28 200 K to 8600 K in the atmosphere at argon 12 Torr pressure and, comparing with 17 800 K to 7400 K in a vacuum. The high value of temperature makes the plasma expand faster; consequently, the rate of plasma cooling is faster. As can be seen, the argon atmosphere at 12 Torr produces the highest initial temperature (> 28 200 K at 0.3 μs time delay) and the slowest decay. After 0.9 μs from the laser pulse, the temperature decreases much

slower. The plasmas obtained in a vacuum show a similar temporal behavior, but with a lower temperature at each time. It can be concluded that confinement creates hotter plasmas. It is observed that in the argon atmosphere, although the temperature increases with increasing gas pressure, it decreases with increasing delay.

Determination of the Electron Number Density

One of the most reliable spectroscopic techniques to determine N_e is from the Stark broadening line profiles of a neutral atom or single-charged ion. This technique assumes the Stark effect to be the dominant broadening mechanism. When the density of plasma is $> 10^{15}$ cm^{-3}, Stark broadening is predominant, and Doppler effects, Van der Waals broadening, and resonance broadening can be neglected.[28,32,33] In this work, Stark broadening prevails, resulting from the perturbation of the excited levels of the radiating lead atoms due to collisions mainly with the plasma electrons, whereas other broadening mechanisms are negligible. The theoretical FWHM of a Stark broadened line can be used for the determination of *Ne* using the following equation:[32,33]

$$\omega_S = 2\omega_{exp}\left(\frac{N_e}{10^{16}}\right)\left[1 + 1.75A\left(\frac{N_e}{10^{16}}\right)^{1/4}\left(1 - 1.2{N_D}^{-1/3}\right)\right] \quad (3)$$

where $\omega_S(=\Delta\lambda_{\frac{1}{2}})$, in Angstrom units, is the FWHM of the transition considered and obtained at the density N_e expressed in cm^{-3}. The coefficients ω_{exp} and A, both independent of density and weak functions of temperature, are the electron impact-width parameter and the ion-broadening parameter, respectively. The parameter N_D is the number of particles in the Debye sphere, which must be in excess of the lower limit $N_D = 2$ of the Debye approximation for correlation effects.[43] For the electron densities present in this study, the quasi-static ion broadening, taken into account in the second term in Eq. 3, is only approximately 5% of the total width. In our measurements, we have assumed that A is negligible (Konjević[34]); therefore, the determined N_e can be obtained with the following equation:

$$N_e = \left(\frac{\omega_S}{2\omega_{exp}}\right) \times 10^{16}(cm^{-3}) \quad (4)$$

The electron number density, N_e (cm^{-3}), of the plasmas investigated has been extracted by comparing the ω_S(FWHM), in Å, of several lines Pb(I), Pb(II), and Pb(III), and line 4348.1 Å of Ar(II) obtained in this work with those ω_{exp} values (at different temperatures and electron number densities) from other authors that are presented in Table II.[13,24,25,28,44] These electron densities have been estimated to an accuracy of 10–20%; error is essentially due to uncertainties of the used Stark broadening parameters. As already mentioned in obtaining the temperature, different spectral lines have been used in each time delay. In a vacuum, the spectral lines 3854.08 Å, 3689.31 Å, and 3729.69 Å of Pb(III) have been used at short time delays (0.3 μs, 0.4 μs) and the spectral lines 3639.57 Å and 3739.99 Å of Pb(I) and spectral lines 3785.99 Å, 3718.30 Å, and

Table II. Stark width FWHM, ω (Å), of Pb(I), Pb(II), Pb(III), and Ar(II) spectra lines using in the determination of electron number densities.

Specie	Transition	λ (Å)[a]	T ($\times 10^3$)K	*Ne* (cm^{-3})	ω_{exp} (Å)
Pb(I)					
	$5d^{10}6s^26p\ (^2P_{1/2})\ 7s\ ^3P_1 \rightarrow 5d^{10}6p^2\ ^3P_1$	3639.57	11.2	1.0×10^{17}	0.15 ± 0.01[b]
	$5d^{10}6s^26p\ (^2P_{1/2})\ 7s\ ^3P_2 \rightarrow 5d^{10}6p^2\ ^1D_2$	3739.99	11.2	1.0×10^{17}	0.11 ± 0.01[b]
Pb(II)					
	$5d^{10}6s^2\ (^1S)\ 5f\ ^2F_{5/2} \rightarrow 5d^{10}6s^2\ (^1S)\ 6p^2\ ^4P_{3/2}$	3785.99	11.3	1.0×10^{16}	0.18 ± 0.03[c]
	$5d^{10}6s^2\ (^1S)\ 9s\ ^2S_{1/2} \rightarrow 5d^{10}6s^2\ (^1S)\ 7p\ ^2P_{1/2}$	3718.30	11.3	1.0×10^{16}	0.33 ± 0.03[c]
	$5d^{10}6s^2\ (^1S)\ 8d\ ^2D_{5/2} \rightarrow 5d^{10}6s^2\ (^1S)\ 7p\ ^2P_{1/2}$	3713.98	11.3	1.0×10^{16}	0.41 ± 0.06[c]
Pb(III)					
	$5d^{10}6s\ (^2S)\ 7p\ ^3P_2 \rightarrow 5d^{10}6s\ (^2S)\ 7s\ ^3S_1$	3854.08	21.4	1.0×10^{17}	0.82 ± 0.12[d]
	$5d^{10}6s\ (^2S)\ 7p\ ^1P_1 \rightarrow 5d^{10}6s\ (^2S)\ 7s\ ^3S_1$	3689.31	21.4	1.0×10^{17}	0.69 ± 0.11[d]
	$5d^{10}6s\ (^2S)\ 8s\ ^3S_1 \rightarrow 5d^{10}6s\ (^2S)\ 7p\ ^3P_1$	3729.69	21.4	1.0×10^{17}	0.94 ± 0.14[d]
Ar(II)	$3s^23p^4\ (^3P)\ 4p\ ^4D_{7/2} \rightarrow 3s^23p^4\ (^3P)\ 4s\ ^4P_{5/2}$	4348.1	15.0	1.0×10^{17}	0.24 ± 0.02[e]

[a]Moore.
[b]Alonso-Medina.
[c]Colón and Alonso-Medina.
[d]Alonso-Medina.
[e]Aparicio et al.

3713.98 Å of Pb(II) have been used at long time delays (0.6–6.5 μs). In the argon atmosphere, the spectral line 4348.1 Å of Ar(II) has been used at short time delays (0.3–0.6 μs) and the spectral lines 3639.57 Å and 3739.99 Å of Pb(I) and spectral lines 3785.99 Å, 3718.30 Å, and 3713.98 Å of Pb(II) have been used at long time delays (0.9–6.5 μs).

The temporal evolution of the electron number density of laser lead plasma generated in the three atmospheres (vacuum and argon at 6 Torr and 12 Torr) versus delay times is shown in Figure S1; Figures S1–S6 show the electron density measurement error of about 10–15% indicated by vertical error bars. It is observed that the electron density decreases exponentially with the delay times, decreases rapidly until 0.6 μs and then slowly after 0.8 μs, in the three atmospheres. In the argon atmosphere at 6 Torr, was found that the values of the electron densities decrease in the range of 0.75×10^{17} cm^{-3} to 0.3×10^{16} $cm–^{3}$, for time delays 0.4–6.5 μs. As can be seen, the argon atmosphere at 12 Torr produces the highest initial electron number density 1.3×10^{17} cm^{-3} at time delay 0.3 μs and that, for example, at 1.5 μs in a vacuum the value is 1.0×10^{16} cm^{-3}, in argon at 6 Torr it is 1.8×10^{16} cm^{-3}, in argon at 12 Torr it is 2.1×10^{16} cm^{-3}, and in argon at 24 Torr it is 3.0×10^{16} cm^{-3}. These results indicate that the electron number density at the initial stage is very high and decreases quickly with time. Thus, the higher electron number density in the argon atmosphere is assumed to be primarily the result of the higher plasma temperature under the argon atmosphere and that in a vacuum decaying faster than argon.

For time delays 0.15 μs and 0.2 μs, N_e and T_e have not been studied since the spectral lines are absorbed; the plasma never reach the LTE conditions.

Existence of Local Thermodynamic Equilibrium

For the plasma to be in LTE, atomic and ionic states should be populated and depopulated predominantly by collisions rather than by radiation. This requires the electron density to be high enough to ensure a high collision rate. The corresponding lower limit of N_e is given by McWhirter's criterion:[43,45]

$$N_e(cm^{-3}) \geq 1.6 \times 10^{12} \sqrt{T}(E)^3 \quad (5)$$

where T_e (in K) is the temperature, ΔE (in eV) is the energy difference between the upper and lower strongly radiatively coupled states which are expected to be in LTE and N_e is the lower limit in the electron density to collision maintain the energy level populations to within 10%[43] of LTE while competing with radiative processes. For example: (1) using the values obtained of the spectral lines of Pb(II) (at delay time 1.5 μs, in vacuum, $\Delta E_i = 2.599$ eV and 13 080 K) the value *Ne* by McWhirter's criterion is 3.21×10^{15} cm^{-3} against the value obtained 1×10^{16} cm^{-3}; and (2) using the values obtained of the spectral lines of Ar(II) (at delay time 0.3 μs, in 6 Torr argon atmosphere, $\Delta E_i = 2.269$ eV and 24150 K) the value N_e by McWhirter's criterion is 2.90×10^{15} cm^{-3} against the value obtained 9×10^{16} cm^{-3}. In this work, it has been verified that during the plasma expansion (between 0.3–6.5 μs time delays), McWhirter's criterion is met.

The McWhirter criterion is considered a necessary condition, but not sufficient for the existence of LTE in the plasma-generated laser, to define a minimum electron density.[21,34–36,40] In this work, the existence of LTE has been corroborated by comparing the electron number density directly measured with the Stark effect with the corresponding values obtained using the Saha equation. A detailed study is presented in Cristoforetti et al.,[35] i.e., the use of the Saha equation and the measurement of the Stark broadening of a suitable transition in the observed lines has provided us with a reliable way to corroborate LTE. In the Saha equation, only intensity of two emission lines of the different ionization level and T_{ex} need to be known. It was observed that the Saha equation generated a slightly higher electron number density value than with the Stark effect, but within the experimental uncertainty range, see for example in an argon atmosphere at 6 Torr and time delay 0.6 μs the electron number density obtained was: (1) 0.53×10^{17} $cm^{-3} \pm 10\%$ with the Stark effect; and (2) 0.60×10^{17} $cm^{-3} \pm 15\%$ with the Saha equation.

All values for N_e and T_e measured in this work correspond to the center of the plasma. To determine the change of these parameters in different regions of the plasma, that is, to study the homogeneity of the plasmas measured in this work, we have obtained their values in different points of the plasma by using several Pb(I), Pb(II), Pb(III), and Ar(II) lines and in different conditions (different atmospheres and time delays) following the process described above, in the experimental setup and details of the measurements. The results indicate a satisfactory homogeneity for N_e and T_e. In a region far from the center of the plasma corresponding to approximately 95% of the total light emission, deviations from the average are $< 13\%$ for N_e and $< 6\%$ for T_e. The consistency of N_e from the lines of two ionization stages indicates that the lines are emitted from the same region of plasma.[34] Similar results for the *Ne* and *T* homogeneity have been found in other LIP experiments.[13,22–29]

Analysis of the Stark Widths and Shift of the 2203.5 Å and 4386.5 Å Pb(II) Spectral Lines

Stark widths and shift of spectral lines in plasmas is determined by two factors: the plasma environment and the atomic structure of the emitting atom or ion. The calculations of Stark broadening are described in the references;[32,46] because of the complexity of these calculations,

there is a great need for accurate measurements under well-defined conditions. The theoretical full half-width, $\omega_t(N_e, T_e)$, and shift, $d_t(N_e, T_e)$, of singly ionized atom lines obtained by means of equations described in Griem,[32] also present as Eqs. 6 and 7 in the work of Konjević et al.,[47] may be calculated from data collected in Griem.[32] Shifts are usually, but not always, to longer wavelengths redshift, they appear to be due to changes in the relative positions of perturbing levels, because close interacting levels tend to be above the upper level of the line, rather, than below that is to say it is mostly attributed to their level states and the quadratic Stark effect. The Stark effect phenomenon in plasmas is due to the collisions of the emitting atoms/ions with electrons and ions. The electric field generated by these electrons/ions in the plasma perturbs the energy levels of the individual atoms/ions, thereby broadening the resultant emission lines. This perturbation is also unsymmetrical in nature, hence there will be small shifts of the intensity maxima of line profiles. If the shifts are relatively small in terms of line widths, they may also be strongly temperature-dependent. This effect can be traced to cancellation of different perturbing levels. It may even lead to a change in the sign of the shift, as observed in this work.

In this work, the results of an experimental study of Stark widths and shift of 2203.5 Å and 4386.5 Å of Pb(II) emission lines as a function of obtained electron density and temperature, studied in different atmospheres and time delays, are presented. The line shift is primarily caused by the Stark effect so the energy level can be obtained by analyzing the corresponding line shift. The departure energy level of line 2203.5 Å is 59 448 cm^{-1} and of line 4386.5 Å is 92 529 cm^{-1}, being the ionization limit energy 121 243 cm^{-1} of Pb(II) (see Pb(II) partial Grotrian diagram in Fig. 1 based on Colon and Alonso-Medina[16]). The Stark widths and shift were gained at every delay time and different ambient condition. The intensities of these spectral lines begin with an increasing dependence on delay times, continued by a decrease, as shown in Figs. 1 and 2, giving us information about the density of the atoms in each excited state. The dependence of the Stark widths, ω_S, and shift, d, of the line maximum with plasma parameters (N_e and T_e) is very explicit and has been proved in a number of experiments made by different authors. Only if observed line shapes are indeed symmetrical can shifts be defined easily. In order to illustrate line shape and shift of the Stark broadening obtained in this work, see Figs. S2–S4 in the Supplemental Material.

Figures S2–S4 show the emission spectrum of lead plasma covering the spectral region 4335–4425 Å, in the argon atmosphere at different pressures of 6 Torr, 12 Torr, and 24 Torr, respectively, and at different time delays. The Stark width lines are much larger at the early stage, see 0.4 μs and 0.6 μs, than in the final stage; the time delay is longer, see 1.5 μs and 2.5 μs. In the spectral lines 2203.5 Å (second order) and 4386.5 Å of Pb(II), it has already been shown (Fig. 4) that a delay time of 0.8 μs presents self-reversal and shift. The reason is that the profile of the line is governed by the collision of the emitting atoms with ions and electrons. There are a lot of electrons, excited atoms, and ions in the initial plasma which would enhance the possibility of collisions between the free electrons and excited atoms or ions. When the delay time increases, the plasma could be regarded as the equilibrium state in which probability of collision becomes very small.

There are also obvious shifts in these spectral lines in the argon atmosphere at different pressures and at different delay times. The evolution of the lines shift has been illustrated in Fig. S2b and c, at 6 Torr, respectively; in Fig. S3a and b at 12 Torr; and in Fig. S4a and b at 24 Torr. In Fig. S2b, a redshift in spectral line 2203.5 Å (second order) of Pb(II) is noticed, at time delays (see 0.4 μs, 0.6 μs, 1.5 μs, and 2.5 μs), and in Fig. S2c, a blueshift in spectral line 4386.5 Å of Pb(II) can be seen, at a short time delay (see 0.4 μs and 0.6 μs) and redshift time delay longer (see 1.5 μs and 2.5 μs). In Fig. S3a and b, a redshift can be observed at different delay times, for said lines. In Fig. S4a and b, a redshift can be noticed towards the time delays of 1.5 μs, 2.5 μs, and 4.5 μs, and a blueshift at the time delay of 6.5 μs in spectral line 4386.5 Å of Pb(II). On the other hand, for the line 2203.5 Å (second order) of Pb(II), the shift is toward the red in all delays. At shorter delay times, as pressure increases of argon increased self-absorption produces poorer peak resolution and is difficult to quantify because the shape of the peak can be misleading and it is this, as already mentioned above, sufficient reason not to give values the Stark width and shift of line 2203.5 Å and line 4386.5 Å of Pb(II) in an argon atmosphere at 24 Torr, in this work. The line shift is caused by the Stark effect primarily, so the energy level offset can be obtained by analyzing the corresponding line shift. Redshift indicates that the offset of the lower level is smaller than that of the upper level. The results are in agreement with theoretical predictions.

The line shift may be determined at the maximum of the line profile or at its half-width. In this work, it has been determined at the maximum of the line profile. Shift at the peak of line d is usually red (toward larger wavelengths with respect to the unperturbed), but in some cases may be blue, as already mentioned; it is mostly attributed to their level states and the quadratic Stark effect.[46,47] For the measurements of the shifts, the spectral position of a line, the 4348.1 Å of Ar(II), on lead plasma was taken as a reference, because it can be seen that the line 4348.1 Å of Ar(II) was not shifted and was non-self-absorbed during plasma evolution and in the different experimental conditions. As is known, the line shift measurements are most accurate if one can use the same unshifted line for comparison.[34]

Figure S5 shows the emission spectrum of lead plasma covering the spectral region 4335–4425 Å in a vacuum and

Table III. Parameters of the Stark broadening, FWHM, w_S (pm), and shift, d (pm) of the Pb(II) 2203.5 Å spectral line vs. dependence on the electron temperature and the electron density, obtained in lead plasma generated laser in different atmospheres, argon (6–24 Torr), and vacuum at different time delays.

	Time delay (μs)	*Te* (10^3K) ± 10%	*Ne* (10^{17} cm^{-3}) ± 10%	ω_S (pm)	*d* (pm)[a]
Argón atmosphere					
6 Torr					
	0.4	20.6	0.75	4.0 ± 0.5	0.92 ± 0.09
	0.6	18.8	0.53	2.8 ± 0.3	0.63 ± 0.065
	1.5	14.2	0.18	1.1 ± 0.1	0.25 ± 0.03
	2.5	11.6	0.12	0.70 ± 0.08	0.18 ± 0.02
	4.5	9.2	0.05	0.30 ± 0.04	0.08 ± 0.01
	6.5	8.0	0.03	0.24 ± 0.02	0.07 ± 0.01
12 Torr					
	0.3	28.2	1.3	6.9 ± 0.8	1.65 ± 0.10
	0.4	24.0	1.1	5.6 ± 0.6	1.35 ± 0.15
	0.6	21.7	0.71	3.6 ± 0.4	0.85 ± 0.08
	1.5	15.2	0.21	1.0 ± 0.1	0.25 ± 0.02
	2.5	12.3	0.14	0.9 ± 0.1	0.13 ± 0.01
	4.5	9.8	0.063	0.50 ± 0.05	0.11 ± 0.01
	6.5	8.6	0.05	0.31 ± 0.03	0.13 ± 0.01
24 Torr					
	1.5	16.3	0.3	1.3 ± 0.1	0.35 ± 0.04
	2.5	13.2	0.16	0.8 ± 0.1	0.21 ± 0.02
	4.5	10.0	0.07	0.47 ± 0.05	0.12 ± 0.01
	6.5	9.0	0.06	0.40 ± 0.04	0.10 ± 0.01
Vacuum					
	0.4	17.8	0.48	2.4 ± 0.3	–(0.45 ± 0.04)
	0.6	16.2	0.25	1.1 ± 0.1	–(0.30 ± 0.03)
	0.8	15.5	0.2	0.91 ± 0.09	–(0.21 ± 0.02)
	0.9	14.8	0.17	0.84 ± 0.08	–(0.25 ± 0.02)
Djeniže et al.					
Colón and Alonso-Medina	28.0	1.9	9.4 ± 25%	0.0	
	11.3	0.1	11.0 ± 10%		
Colón and Alonso-Medina	11.6	1	12.5		

[a]The positive shift is toward longer wavelengths (red).

different delay times. Figure S5b shows that the spectral line 4386.5 Å of Pb(II) is blueshifted at a short time delay (see 0.4 and 0.6 μs) and that there are also shifts to the blue of the resonant spectral line 2203.5 Å (second order) of Pb(II). In a vacuum, the line 4348.1 Å of Ar(II) is not available for checking. Line 2170.0 Å (second order) of Pb(I) has been used after checking so that it does not move under the conditions of study.

Tables III and IV list the Stark widths (ω_S) and shifts (d) experimentally determined for the investigated 2203.5 Å and 4386.5 Å spectral lines of singly ionized lead in different delay times, respectively. The Stark width FWHM, ω_S(pm), and shifts, d (pm), are displayed in columns 5 and 6, respectively. Column 1 of Tables III and IV lists the different atmospheres, column 2 lists the delay times, and columns 3 and 4 list the temperature and electron number density, respectively. Finally, in the last rows of these tables presented the values obtained by other authors are presented, both experimental and theoretical, and good agreement is seen. The important effect of the different environment where the plasma expands has been pointed out.

It is well known that knowledge of the Stark width and shift values and the electron density is very useful in plasma diagnostics. Stark parameter dependence on the electron density is well established in the case of non-hydrogenic emitters. Stark width dependence is essentially linear, although the deviation from this linear dependence is to be expected beyond some density, depending on the line

Table IV. Parameters of the Stark broadening: width FWHM, ω_S (pm), and shift, d (pm) of the Pb(II) 4386.5 Å spectral line versus dependence on the electron temperature and the electron density, obtained in lead plasma generated laser in different atmospheres, argon (6–24 Torr), and vacuum, at different time delays.

	Time delay (μs)	*Te* (10^3K) ± 10%	*Ne* (10^{17} cm^{-3}) ± 10%	ω_S (pm)	*d* (pm)[a]
Argón atmosphere					
6 Torr					
	0.4	20.6	0.75	64.2 ± 6.4	17.5 ± 1.8
	0.6	18.8	0.53	50.3 ± 5.0	14.8 ± 1.5
	1.5	14.2	0.18	21.4 ± 2.1	−(2.0 ± 0.2)
	2.5	11.6	0.12	16.5 ± 1.7	−(3.4 ± 0.3)
	4.5	9.2	0.05	12.2 ± 1.2	−(3.1 ± 0.3)
	6.5	8.0	0.03	8.9 ± 0.08	−(2.2 ± 0.2)
12 Torr					
	0.3	28.2	1.3	92.6 ± 9.3	28.2 ± 2.8
	0.4	24.3	1.1	80.4 ± 8.0	23.5 ± 2.3
	0.6	21.8	0.71	55.4 ± 5.5	18.3 ± 1.8
	1.5	15.2	0.21	18.5 ± 1.9	6.4 ± 0.6
	2.5	12.3	0.14	14.2 ± 1.4	5.1 ± 0.5
	4.5	9.8	0.063	9.1 ± 0.9	2.7 ± 0.3
	6.5	8.6	0.05	8.4 ± 0.8	2.2 ± 0.2
24 Torr					
	1.5	16.3	0.3	22.0 ± 2.2	7.5 ± 0.8
	2.5	13.2	0.16	18.3 ± 1.8	5.6 ± 0.7
	4.5	10.0	0.07	10.5 ± 1.1	3.6 ± 0.4
	6.5	9.0	0.06	9.5 ± 0.9	−(0.1 ± 0.01)
Vacuum					
	0.4	17.8	0.48	36.3 ± 3.6	−(10.0 ± 1.0)
	0.6	16.2	0.25	20.4 ± 2.0	−(6.5 ± 0.7)
	0.8	15.5	0.2	20.0 ± 2.0	−(6.2 ± 0.6)
	0.9	14.8	0.17	21.0 ± 2.1	−(7.0 ± 0.7)
Miller et al.					
Djeniže et al.	11.6 ± 1.0	1.0	172 ± 20%		
Fishman et al.	27.0	1.62	51 ± 30%	15.1 ± 30%	
Colón and Alonso-Medina	24.0	1.0	70 ± 30%		
	11.3	0.1	13.0 ± 10%		

[a]The positive shift is toward longer wavelengths (red).

in the study.[46] This work and the lines under study corroborate this linear dependence. However, the dependence on the temperature is different for each line of each spectrum, instead of the commonly adopted temperature dependence of $\sim T^{-1/2}$ for ion lines, as seen in this work. Tables III and IV present many values of the Stark parameters of the lines under study to allow us to see these dependencies. Figure S6, for example, shows the dependence of the Stark width and shift with the electron density and electron temperature for the Pb(II) 2203.5 Å spectral line. For the spectral line in Fig. S6a and b, respectively, the expected linear dependence (with zero intercept) of Stark width and shift with the electron density both for redshift and for blueshift is noted. In Fig. S6c and d, respectively, the dependence of Stark width and shift with the electron temperature is noted.

Conclusion

In this article, we presented the results of an experimental study of Stark broadening of 2203.5 Å and 4386.5 Å spectral lines of Pb(II).

The evolution of the plasmas was studied by acquiring spectra at several time delays (0.15–9 μs after the laser pulse). There has been a set of experiments to study the effect of the ambient environment on the resolution of the

peaks, the S/N intensity, the emission intensity, and also on the different parameters of plasma obtained. It is concluded that: (1) in a vacuum the plasma expands freely, the emissivity of lines can last for up to several microseconds, plasma evolution is fast, and LTE is easier to obtain in the final stages of evolution than in the early stages; and (2) in the presence of a controlled argon atmosphere, rates of recombination and collision excitation of plasma species were increased, the cooling rate was enhanced, and hence the emission intensities were increased. The pressure of the ambient atmosphere is one factor of the controlling parameters of the plasma characteristic.

The LTE assumption is discussed and self-absorption effects were determined as well. The use of emission spectroscopy for the measurement of temperature and electron density of the plasma requires optically thin spectral lines. We reported the measurements of electron density and plasmas temperature at the different delay times. For large delays, $> 1\ \mu s$, we observed the plasma in LTE, for- $< 0.3\ \mu s$, accurate LIBS measurements require the consideration of the non-uniform spatial distributions of temperature and electron density.

The study of the temperatures as a function of delay time provides interesting information on the species living in the plasma. The temperature decreases rapidly with plasma expansion, inducing recombination and decreasing the number of heavy particles (atoms and ions). We have demonstrated that electron number density and plasma temperature decrease exponentially as the delay time increases due to plasma expansion and the exchange of energy, i.e., as a consequence of the expansion and of the exchange of energy with the surrounding environment, the electron number density and the excitation temperature strongly decrease on short delay time. Electron temperatures were measured in the range of 8000–20 600 K at an argon atmosphere at 6 Torr pressure, 8600–28 200 K at an argon atmosphere at 12 Torr pressure, and 7400–17 800 K under a vacuum. Electron densities in the range of 0.03×10^{17} cm^{-3} to 0.75×10^{17} cm^{-3} in an argon atmosphere at 6 Torr pressure, 0.05×10^{17} cm^{-3} to 1.3×10^{17} cm^{-3} at an argon atmosphere at 12 Torr pressure, and 0.01×10^{17} cm^{-3} to 0.48×10^{17} cm^{-3} under a vacuum were observed. The results show that the expansion velocities of the plasma, the electron temperature, and the electron density are all influenced by the environment. The expansion velocities in a vacuum pass from an initial velocity of around 10^{6} cm^{-1} to 8×10^{5} cm^{-1} after a few microseconds and in an argon atmosphere pass from an initial velocity of around 10^{6} cm^{-1} to 4×10^{5} cm^{-1}. Thus, the higher electron number density in an argon atmosphere is assumed to be primarily the result of the higher plasma temperature under argon atmosphere and that in vacuum decays faster than argon.

The Stark widths and shift of 2203.5 Å and 4386.5 Å of Pb(II) emission lines were detected and has been measured (with $\pm$ 10% error) as a function of electron density and temperature obtained in different atmosphere and different time delays. Contributing, in this work, with more precise values than those measured by other authors, and for the shift of 2203.5 Å the first measures that are presented in the literature The redshift and blueshift, *d*, are encountered and appear to be readily explainable in terms of special circumstances in the plasma environment and in the atomic structure. The Stark shifts may still be very useful for plasma diagnostic.

The expected linear dependence of Stark parameters on the electron density is explored in this work for two Pb(II) 2203.5 Å and 4386.5 Å spectral lines in study as well as its dependence and regularity with temperature.

Conflict of Interest

The authors report there are no conflicts of interest.

Funding

This work has been supported by the Spanish DGI project MAT2015-63974-C4-2-R.

Supplemental Material

All supplemental material mentioned in the text, consisting of Figs. S1–S6, is available in the online version of the journal.

ORCID iD

Aurelia Alonso Medina http://orcid.org/0000-0002-7460-6561